Transparency Engineering in Quantum Dot-Based Memories

Ismail Firat Arikan, Nathanaël Cottet, Tobias Nowozin, and Dieter Bimberg*

Quantum dot (QD) based memories offer new functionalities as compared to present main stream ones by combining the advantages of DRAM (fast access and write/erase time, good endurance) and Flash memories (long storage time). The present storage times in such memories are demonstrated to be several days at room temperature for GaP-based devices, while write times as short as picoseconds are possible. There exists however a trade-off between storage time and erase time. To eliminate this trade-off, resonant tunneling effects in single or double quantum well structures are studied here as a promising approach. The quantum well structures based on GaAs/$Al_{0.9}Ga_{0.1}As$ and GaP/AlP quantum wells inserted in QD-based memories are designed and simulated using a Schrödinger-Poisson solver and non-equilibrium Green's functions (NEGF) to calculate the transparency at a given voltage. By choosing the width of the quantum wells, precise positioning of their energy levels allows for transparency engineering. Our simulations show an increase in transparency by at least 7 orders of magnitude at resonance, leading indeed to sufficiently fast erase times, thus solving the trade-off problem.

1. Introduction

The semiconductor memory market is currently dominated by complementary Flash and Dynamic Random Access Memories (DRAMs). In Flash memories, the charge carriers are confined between two SiO_2 barriers having a height of 3.2 eV, which allows storage times of more than 10 years. However, this barrier height prevents fast write/erase times and good endurance (only 10^6 write/erase cycles are possible) due to the creation of defects as a

I. F. Arikan, Dr. T. Nowozin, Prof. D. Bimberg
Institut für Festkörperphysik
Technische Universität Berlin
Hardenbergstr. 36, 10623 Berlin, Germany
E-mail: ifarikan@mailbox.tu-berlin.de

N. Cottet
Ecole Normale Superieure
International Center of Fundamental Physics
Paris, France

Prof. D. Bimberg
Changchun Institute of Optics
Fine Mechanics and Physics, CAS
Beijing, China

The ORCID identification number(s) for the author(s) of this article can be found under https://doi.org/10.1002/pssa.201800018.

result of injection of hot electrons into the floating gate.[1] Using a capacitor, DRAM reaches write/erase times of 15 ns and an endurance of 10^{15} write/erase cycles, but at the cost of a small retention time (around 10 ms). An ideal memory should combine the advantages of both types, while remaining scalable. Such a memory could revolutionize computer architectures.[2] This goal remains difficult to achieve because of the large difference between an ideal storage time (more than 10 years) and an ideal erase time (less than 1 ns).

Memory units based on III–V self-organized quantum dots (QDs),[3] for example InAs/GaAs QDs, appear as a promising approach, because the barrier height is tunable,[4,5] in contrast to other semiconductor memory concepts. The charge carriers are confined here in the QDs. Hole storage offers significant advantages as compared to electron storage because the energy levels of confined holes are much more closely spaced than those of electrons due to their larger effective mass. Thus, at least one order of magnitude more holes can be stored in a given volume than electrons. In addition carrier escape is strongly reduced due to their one order of magnitude larger effective mass.

A typical QD memory structure is made of a single QD layer coupled through a tunnel barrier to a two-dimensional hole gas (2DHG) which acts as a hole reservoir. The read-out of the stored information is done by conductance measurements of the 2DHG: carriers stored in the QDs reduce the charge density and the mobility in the 2DHG. To store a *logic 1*, defined as populated QDs, an emission barrier is needed to prevent holes from escaping. This barrier is given by the localization energy of the QDs. To store a *logic 0*, defined as empty QDs, a capture barrier is needed to prevent holes from being captured by QDs and is provided by the band bending of the Schottky contact. Writing and erasing are achieved by applying a gate voltage. A bias in forward direction is applied to the gate to fill the QDs. This completely eliminates the capture barrier (flatband condition) and very fast write times can be realized: the holes are captured with times of the order of ps at room temperature.[6,7] Applying a bias in reverse direction narrows the emission barrier and the emission probability increases, so that tunnel emission is induced.[8]

However, the trade-off between storage and erase time remains a challenging problem to solve. To understand precisely the trade-off between long storage times and fast erase times, it is

necessary to know how holes are emitted from the QDs.[9,10] Neglecting optical effects, there are three possible emission processes: thermal emission, tunnel emission, and thermally-assisted tunneling. Thermal emission occurs when the thermal energy of the holes is sufficient to overcome the emission barrier E_A (called localization energy of the QD).[11–13] The thermal emission rate at a temperature T is given by

$$e^{\mathrm{TH}} = \gamma T^2 \sigma_\infty \exp\left(-\frac{E_a}{k_B T}\right) \qquad (1)$$

where k_B is the Boltzmann constant, γ a temperature-independent constant, and σ_∞ the apparent capture cross section of the QDs. In QDs with a triangular emission barrier, the tunnel emission rate e^{TUN} depends on the barrier width w and on the external electrical field F (which influences the barrier width). More precisely, the rate is

$$e^{\mathrm{TUN}} = \frac{eF}{4\sqrt{2m^* E_a}} T(\varepsilon_{QD}) \qquad (2)$$

where m^* is the effective mass and $T(\varepsilon_{QD})$ is the transparency at the energy which is the ground state energy of the QDs. Thermally-assisted tunneling represents a two-step process: thermal activation from a lower state of the QD to an excited state, and tunneling through the remaining barrier. To achieve long storage times in QDs at room temperature, a high barrier E_A is needed in order to keep the thermal emission rate low. However, increasing the barrier E_A also leads to a lower tunneling rate, which drastically increases the erase time. Consequently, the erase process remains slow compared to DRAM memories: erase times achieved in actual QD-based memories are still many orders of magnitude larger than the erase time of a DRAM. The only way this trade-off can be eliminated is by introducing a way to switch the transparency T. The barrier has to be designed in such a way that two states exist: a storage state with a very low transparency (long storage time) and an erase state with a very high transparency (short erase time). This new type of barrier can be based on QW structures coupled to the QDs. We derive in this work details of the design of such structures using a Schrödinger Poisson Solver and a Non-Equilibrium Green's Functions (NEGF) approach.

As an alternative to the semiconductor memory devices, ternary data storage devices are suggested to achieve high-density data storage (HDDS). Such memory devices are formed by organic materials instead of inorganic semiconductors and rely on ternary memory states instead of traditional binary systems. Hence, the capacity of the device increases from 2^n to 3^n.[14–16]

2. Resonant Tunneling Heterostructures

Resonant tunneling structures were first used in resonant tunneling diodes.[17,18] Tunneling in a finite superlattice was investigated in the early 1970s by R. Tsu and L. Esaki.[19] They demonstrated the existence of resonances in the tunneling probability (or transparency) through two barriers. The possibility of resonant tunneling through many quantum wells

was proven in the early 1980s and the dependence of the resonant tunneling current on the well number,[20] well widths,[21] and barrier height[22] was studied later on. Transparency engineering in opto-electronic devices was successfully performed in the development of Quantum Cascade Lasers by Faist et al.[23]

The principle of a single/double quantum well structure which shows resonances with a QD at given voltages is represented in **Figure 1**, where the valence band of the superlattice is shown.[24] Resonances occur when the energy of the holes stored in the QDs is equal to an energy level of the quantum well, which means when there is an overlap of the wavefunctions of a state on the left side of the superlattice with the state in the quantum well and a state on the right side of the superlattice. Moreover, it is possible to obtain a resonance through many quantum wells if they share at least one eigenvalue. Because the widths of the quantum wells are different, the energy levels are not at the same position when no bias is applied, which corresponds to the storage configuration (Figure 1a). Applying a voltage tilts the band-structure and shifts the energy levels such that resonance occurs (Figure 1b). At this energy, the transparency of the barriers ideally becomes 1 and the holes tunnel through the superlattice with a probability up to 1.

3. Transparency Calculation

3.1. Non-Equilibrium Green Function Formalism

The tunneling probability of a hole penetrating a tunnel barrier at a given voltage is calculated in two steps. The equilibrium band diagram of the resonant tunnel device at every voltage is calculated from the semiconductor structure using a 1D Schrödinger Poisson Solver.[25] Then, the transparency is calculated from the band diagram in the frame of the Non-equilibrium Green's Functions (NEGF) formalism.[26,27] The domain where we want to calculate the transparency is assumed to be sandwiched between two reservoirs of charge carriers, and the transparency is calculated from one reservoir to the other. With the Hamiltonian H of the structure, the Green's function G is given by
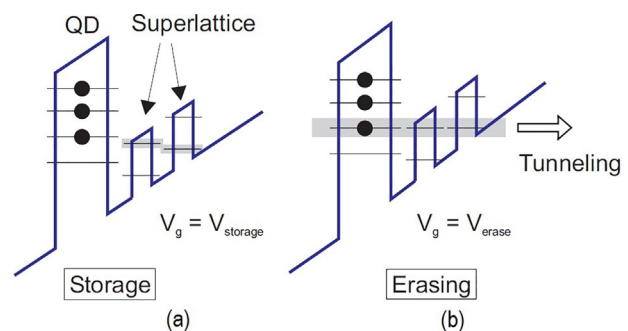
Figure 1. Schematic principle of a resonant tunneling structure for holes (a) out of resonance (storage voltage) and (b) at resonance (erase voltage).

$$G = [EI - H - \Sigma_1 - \Sigma_2]^{-1} \qquad (3)$$

where E is the hole energy, I the identity matrix and $\Sigma_{1,2}$ the self-energy matrices of the contacts, which represent how the structure is coupled to the two reservoirs.[26] Then, the transparency at energy E is given by

$$T(E) = \text{Trace}\left[\Gamma_1 G \Gamma_2 G^\dagger\right] \qquad (4)$$

where $\Gamma_{1,2} = i\left(\Sigma_{1,2} - \Sigma_{1,2}^\dagger\right)$ are the broadening matrices of the contacts. The calculation of the Hamiltonian of the system is straightforward: it is the sum of the free-particle Hamiltonian and the potential profile U calculated by the Poisson-Solver. Using the effective hole mass m^*, the Hamiltonian is given by

$$H = U - \frac{\hbar^2 \nabla^2}{2m^*} \qquad (5)$$

where ∇^2 is the Laplace operator. The use of NEGFs is very convenient in this case because the superlattice structure is considered as a black box placed between two reservoirs. All the information about the structure we need is concentrated in one simple term: U. The other terms remain independent of the superlattice structure.

3.2. Coupling Matrices

For a contact between the continuum and an element with a discrete energy spectrum, the self-energy matrix is

$$\Sigma(E) = \sum_j \frac{|\tau_j|^2}{E - \varepsilon_j + i0^+} \qquad (6)$$

with $|\tau_j|$ coupling energy between the continuum and the energy level ε_j, and 0^+ a regularization constant.[26] Applied to the QD/superlattice contact, where the QD is considered as a one-level element with the energy ϵ_{QD}, it becomes

$$\Sigma_{QD}(E) = \frac{|\tau|^2}{E - \epsilon_{QD} + i0^+} \qquad (7)$$

The self-energy of the 2DHG/superlattice contact is obtained by integration over all the states of the 2DHG. Assuming only one subband to be occupied and using the two-dimensional density of states $D_{2D} = m^*/(\pi\hbar^2)$ we get:

$$\Sigma_{2DHG} = \int D_{2D} \frac{|\tau_\varepsilon|^2}{E - \epsilon + i0^+} d\epsilon \qquad (8)$$

Assuming τ_ϵ independent of the energy ϵ, we obtain the imaginary part of the self-energy:

$$\Im(\Sigma_{2DHG}) = -2\pi D_{2D}|\tau|^2 \qquad (9)$$

The integration process for the real part does not converge, but its effect on the transparency factor is negligible such that the following approximate expression will be used:

$\Sigma_{2DHG} \approx i\Im(\Sigma_{2DHG})$. Unfortunately, the values of the coupling energies are unknown, but we can tolerate this problem as far as we are interested only in the relative variations of the transparency (i.e., between a case with very low transparency and a case with high transparency) and not the absolute values. In the simulations we take $\tau_{QD} = \tau_{2DHG} = 0.05\,\text{eV}$.

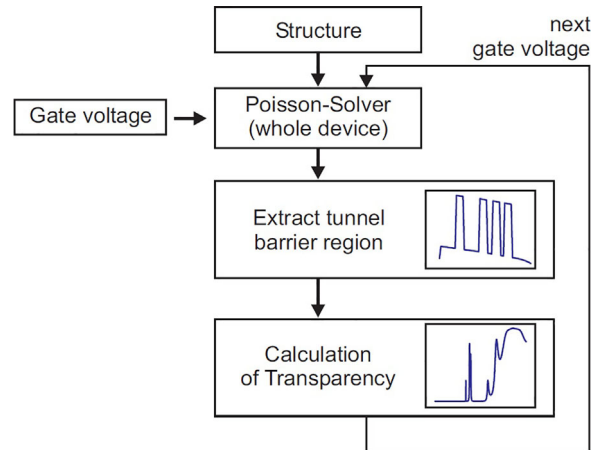### 3.3. Designing the Device and the Calculation Cycle

To design efficient resonant tunneling structures, we chose to represent the evolution of the energy levels of the quantum wells, obtained by diagonalization of the hole Hamiltonian, as a function of the applied voltage. We know that a resonance occurs when the energy levels cross. This point of view is the best way to design such structures because the resonances are easy to locate and because the hole Hamiltonian (including the important potential U) can be calculated very quickly.

Since the tunnel rate is proportional to the transparency $T(\epsilon_{QD})$ at the ground state energy ϵ_{QD} of the QD (see Equation (2)), we only need to calculate the evolution of $T(\epsilon_{QD})$ with the gate voltage V_g to evaluate the effect of the resonant tunneling on the erase time. The schematic calculation used to calculate the transparency-voltage characteristic is shown in **Figure 2**.

At first a structure is designed. Then, its electronic properties such as conduction band, valence band, and doping profile are calculated by 1D Schrödinger-Poisson Solver at a given gate voltage.[28] Afterwards, the resonant tunnel region is extracted from the whole device in order to save computation time by reducing the number of the dash points. Finally, the transparency is calculated by NEGF.

4. Samples

Two different material combinations have been designed: the first group is based on GaAs, while the second group is based on GaP. The reason to choose the GaAs-based material system is, that it has been studied extensively before and is thus very well

Figure 2. Flow diagram of the calculation cycle.

**ADVANCED
SCIENCE NEWS**

www.advancedsciencenews.com

**physica
status
solidi** a

www.pss-a.com

understood. In addition, epitaxial growth of GaAs-based materials is relatively easy. However, it is unlikely that the ultimate goal of 10 years of storage time will be achieved using GaAs-based memories due to the small localization energy of the holes in the QDs. According to both calculations[4,29] and deep level transient spectroscopy (DLTS) measurements,[30,31] GaP-based materials have the potential to achieve non-volatility defined as 10 y storage time. Therefore, GaP-based resonant tunnel structures have been designed.

4.1. GaAs-Based Samples

Four samples have been designed based on GaAs: a sample with one QW, a sample with two QWs, and their reference samples with extra barriers instead of QWs. A schematic of the one-QW GaAs-based sample is shown in **Figure 3**. The basic structure is a modulation-doped field-effect transistor (MODFET) into which the QW is introduced between the QD layer and the 2DHG. We assume a localization energy of 210 meV for holes for InAs QDs embedded in a GaAs matrix, which has been experimentally determined.[32] On the top of an undoped substrate and a 1000 nm nominally undoped GaAs layer, a 40-nm-wide p-doped layer ($p = 1 \times 10^{18}$ cm^{-3}) is introduced to provide holes. After a spacer layer of 7 nm undoped GaAs, the 2DHG is formed in an 8-nm-wide $In_{0.25}Ga_{0.75}As$ QW, on top of which the QW sandwiched between two $Al_{0.9}Ga_{0.1}As$ barriers is placed. The InAs QD layer is placed on top of the QW, separated by 5 nm of undoped GaAs, since the formation of InAs QDs directly on top of an $Al_{0.9}Ga_{0.1}As$ surface would be difficult due to surface roughness. After the QD layer, the device is completed by another 180 nm of undoped GaAs. The 2DHG is contacted via two Ohmic source and drain contacts and the energetic position of the QD hole levels can be tuned by applying a bias voltage to the gate contact.

For the two-QW-sample the superlattice has a similar design, just adding an additional QW and a barrier. To compare the performance with regular samples which do not have a superlattice structure, one reference sample is also simulated for each case. In the reference sample, the GaAs QWs are replaced by $Al_{0.9}Ga_{0.1}As$ barriers, such that a single barrier is formed.

4.2. GaP-Based Samples

Four samples have been designed based on GaP. The structures of the GaP samples are identical to those of GaAs with the differences that GaAs is replaced by GaP, while $Al_{0.9}Ga_{0.1}As$ is replaced by AlP. Also, an InGaSb QD layer is used instead of the InAs QD layer and the 2DHG layer is formed by InP. The localization energy of the InGaSb QDs embedded in the GaP matrix and the energy barrier between GaP and AlP are measured by DLTS. Based on the results of the DLTS measurement, the localization energy of InGaSb QDs used in the simulations is 400 meV, whereas the energy barrier between GaP and AlP is set to 600 meV. Values for the energy barrier between GaP and AlP found in literature vary between 400 and 620 meV.[33] The InGaAs/GaP QD system can be also used as an alternative to the InGaSb/GaP QD system. Stracke et al. demonstrated that the localization energy for $In_{0.25}Ga_{0.75}As$/GaP is 490 meV[34] and Bonato et al. reported that the localization energy for $In_{0.5}Ga_{0.5}As$/GaP is 600 meV.[30] Parameters for the resonant tunnel region for GaP samples are the following: a 5 nm quantum well is sandwiched between two 5 nm wide barriers for the one-QW-sample, two quantum wells whose widths are respectively 6 and 4 nm are sandwiched between three 5 nm wide barriers for two-QW-sample (see **Figure 4**). In the reference samples, the GaP QWs are replaced by AlP barriers.

5. Results

5.1. GaAs-Based Samples

Figure 5a shows the calculated energy levels of the QD and the QW as function of gate voltage for the one-QW-sample. A crossing between the energy levels of the QD and the QW at
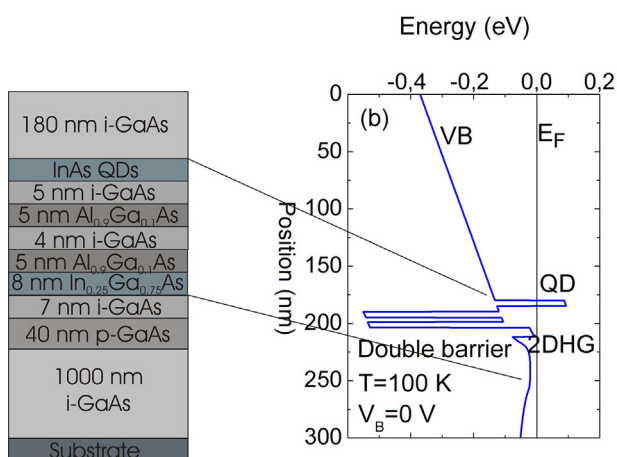
Figure 3. (left) Schematic of a one-QW-sample based on GaAs and (right) its valence band diagram. A two-QW-sample has same design as one-QW-sample, with an additional QW and a barrier.
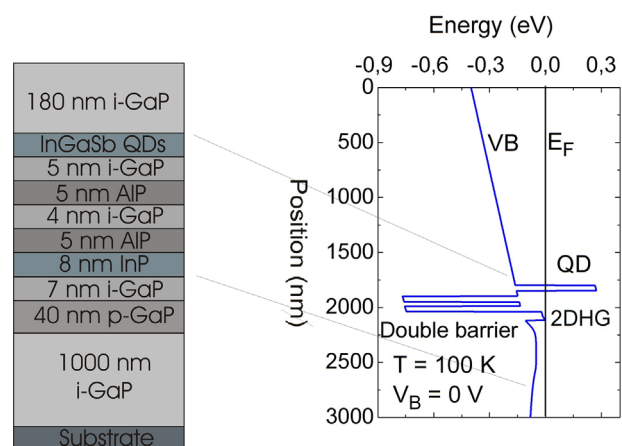
Figure 4. (left) Schematic of a one-QW-sample based on GaP and (right) its valence band diagram. A two-QW-sample has same design as one-QW-sample with an additional QW and a barrier.
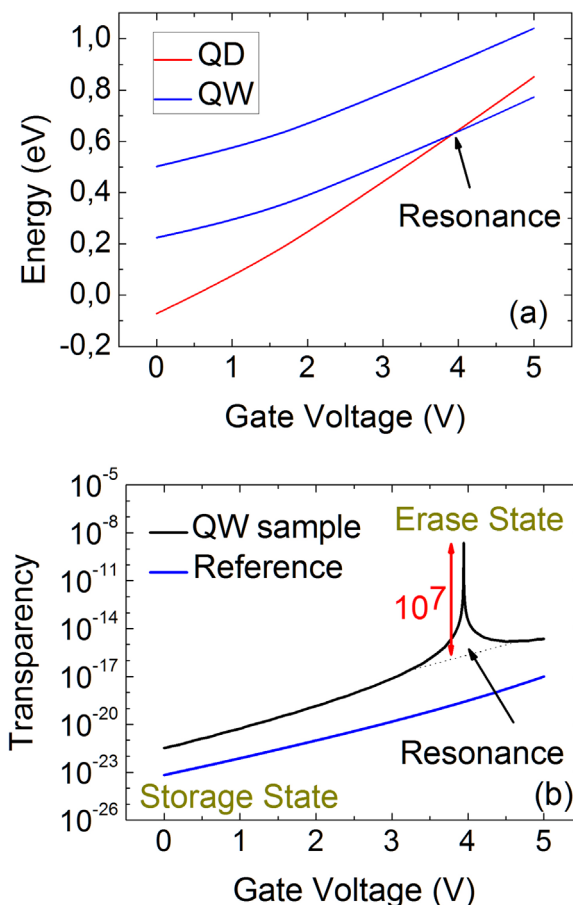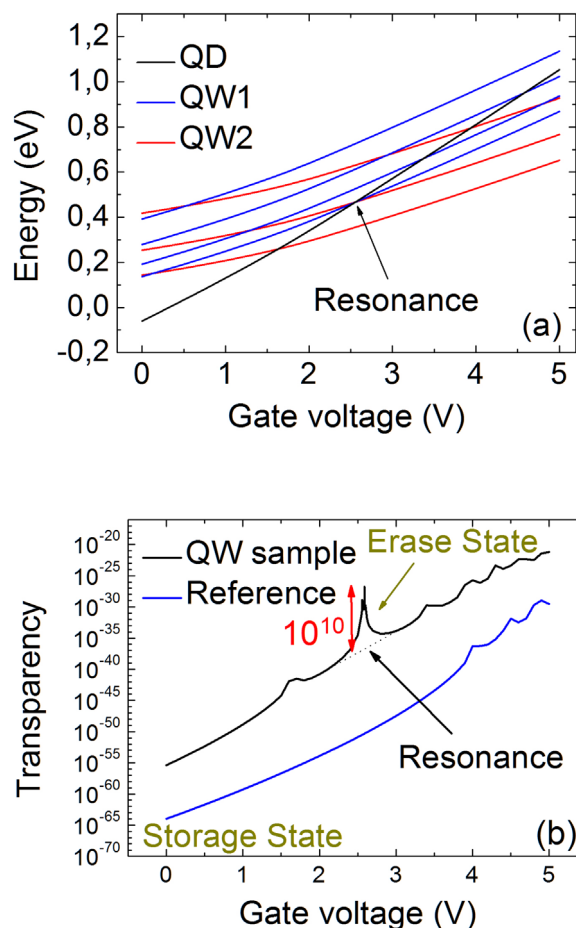
Figure 5. a): The energy levels of the QD and the QW versus gate voltage for the one-QW-sample. There is an intersection point at 3.94V attributed to the resonance. (b): The transparency versus gate voltage for both the one-QW-sample and the reference sample. The transparency increases by 7 orders of magnitude at the resonance voltage for the one-QW-sample, while there is no increase in transparency for the reference sample.
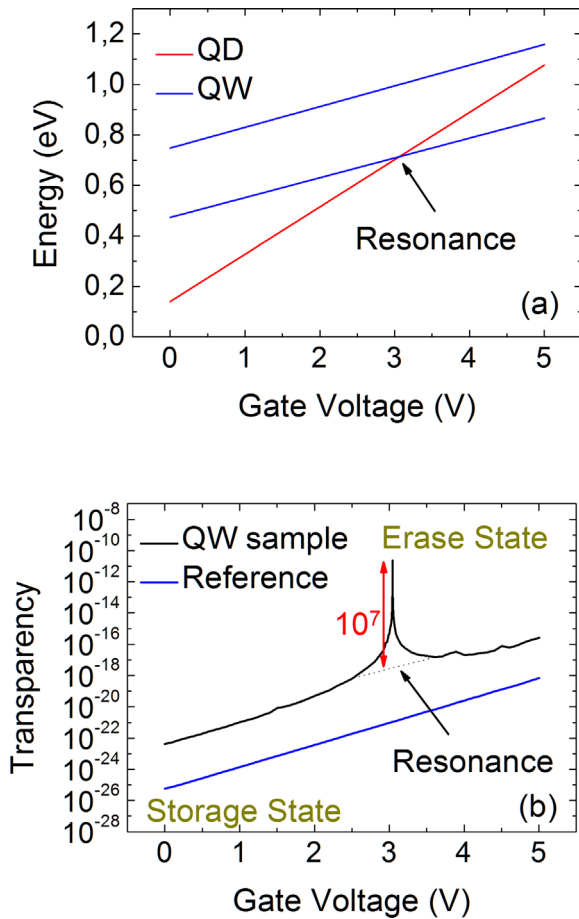
Figure 6. a) The energy levels of the QD and the QWs versus gate voltage for the two-QW-sample. There is one intersection point at 2.56 V attributed to the resonance. (b) The transparency versus gate voltage for both the two-QW-sample and its reference. The transparency increases by 10 orders of magnitude at resonance voltage for the QW-sample, while there is no increase in transparency for the reference sample.

3.94 V can be seen, which represents the alignment between the energy levels throughout the device. An increase by 7 orders of magnitude in the transparency at resonance voltage occurs as shown in Figure 5b. The same figure also shows the transparency for the reference sample. No extra increase in transparency is found for the reference sample. Its transparency increases smoothly with larger reverse bias due to the reduction in barrier height.

It should be noted that deviation of the thickness or composition of the QWs from the ones used here are not changing the calculated transmission coefficient. Small changes of the mentioned parameters result in a small shift of the bias voltage where the resonance is induced.

The calculation shows that an increase in transparency can be achieved by replacing a wide barrier by a QW, thereby realizing orders of magnitude faster erase time since the erase mechanism relies on resonant tunneling.

Figure 6a shows the energy levels of the QD and the QWs for the two-QW-sample. A resonance at 2.56 V can be seen between the QD and two QWs. The transparency for the sample increases

by 10 orders of magnitude at resonance voltage as depicted in Figure 6b. The reference sample shows no increase in transparency.

The challenge for the two-QW-structures is to align all energy levels throughout the whole device, since there is one more energy level due to the additional QW. However, multiple-QW-structures increase the storage/erase time ratio, since the tunneling cannot take place out of resonant voltage resulting in a longer storage time. They also provide the advantage that a thick barrier can be divided into several thin barriers of a given length, hence larger transparency is obtained since the transparency depends strongly on the barrier width.

5.2. GaP-Based Samples

Figure 7a shows the energy levels of the QD and the QW as a function of gate voltage for the one-QW-sample. A resonance between the energy levels of QD and QW at 3.04 V can be seen. At
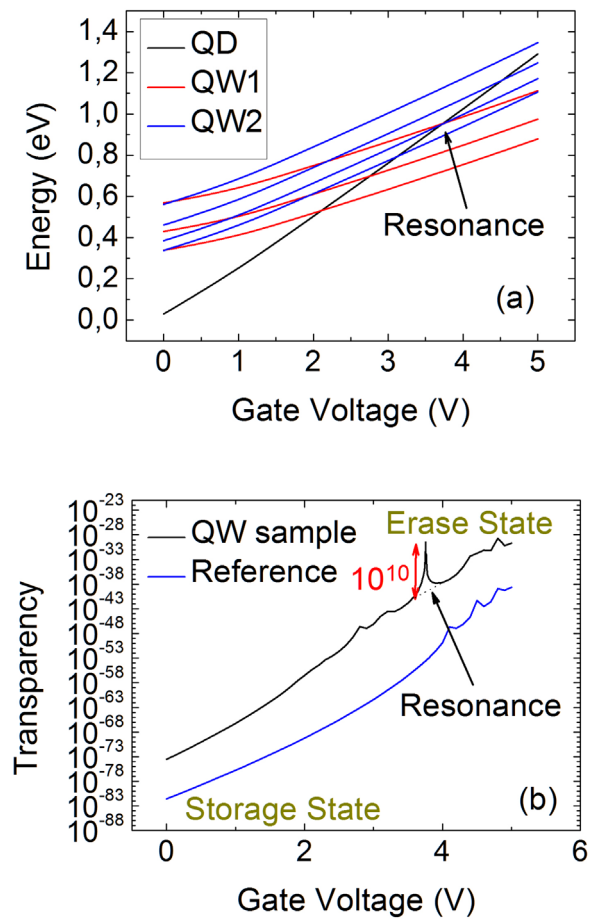
Figure 7. a): The energy levels of the QD and the QW versus gate voltage. There is one intersection point at 3.04 V attributed to the resonance. (b): The transparency versus gate voltage for both the one-QW-sample and its reference. The transparency increases by 7 orders of magnitude at resonance voltage for the QW-sample, while there is no peak in transparency for the reference sample.

Figure 8. a): The energy levels of the QD and the QWs versus gate voltage for the two-QW-sample. There is one intersection point at 2.56 V attributed to the resonance. (b): The transparency versus gate voltage for both the two-QW-sample and its reference. The transparency increases by 10 orders of magnitude at the resonance voltage for the two-QW-sample, while there is no peak in transparency for the reference sample.

the corresponding voltage the transparency increases by 7 orders of magnitude as shown in Figure 7b. The same figure also shows the transparency for the reference sample. No extra increase in transparency is found.

Figure 8a shows the energy level of the QD and the QWs for the two-QW-sample as a function of the voltage. A resonance can be seen at 2.56 V, where the transparency increases by 10 orders of magnitude as shown in Figure 8b. The transparency for the reference sample shows no peak.

6. Discussion

The calculations show that the transparency increases at the resonance voltage, where the energy levels of the QDs and QWs are aligned. For the GaAs one-QW sample, transparency increases by 7 orders of magnitude. The erase times achieved in similar structures without quantum wells are of a few ms.[10] The simulation implies that the implementation of QWs in QD-based memory structures will cause a shortening by 7 orders of

magnitude in erase time. In this case, 1 ns of erase time will be achieved, which is faster than a typical DRAM erase time (10 ns). It should be noted, however, that experimental structures and simulated structures might not exactly be the same, e.g. broadening of the QD energy levels due to a Gaussian distribution of the QD sizes has not been taken into consideration. Nevertheless the increase in the transparency and the decrease in erase time should be of the same order of magnitude. For the two-QW-structures, the increase in transparency is larger than those of the one-QW-sample. Multiple-QW-structures yield the highest storage/erase time ratio.

The simulations for GaP-based samples show that the transparency again increases by 7 orders of magnitude for the one-QW-sample and by 10 orders of magnitude for the two-QW-sample. The simulations prove that the erase time can be decreased by implementation of the QWs into the structure. Besides, the simulations demonstrate that resonant tunneling can be achieved in GaP-based structure, which is presently suggested to be the most promising material combination for non-volatility.

7. Conclusion

In this work, we develop a systematic method of transparency engineering to design resonant tunneling structures for QD-based flash memories, based on energy-voltage calculations and NEGF. By insertion of one or two QWs in QD-based memories, the transparency can be increased at least by 7 orders of magnitude, hence the erase time can be decreased compared to QD-based memories without quantum well for GaAs-based structures. This implies that the 10 ms erase time for an actual structure without superlattice can be reduced to nanoseconds by replacement of the wide barrier with QWs. Furthermore, GaP-based resonant tunneling structures are designed and calculated, confirming it as the most promising material combination to achieve non-volatility. The transparency increases by 7 order of magnitude for the one-QW-sample and 10 orders of magnitude for the two-QW-sample. The results demonstrate that erase times as short as 1 ns can be achieved based on resonant tunneling. Moreover, small changes of the thickness or composition do not affect the transparency coefficient, instead, result in a small shift of the bias voltage, where the resonance is induced. Therefore, the technology of the resonant tunneling memory is stable.

Conflict of Interest

The authors declare no conflict of interest.

[1] R. Bez, E. Camerlenghi, A. Modelli, A. Visconti, *Proc. IEEE* 2003, *91*, 489.
[2] International Technology Roadmap for Semiconductors (ITRS). 2009 Edition, **2009**.
[3] D. Bimberg, M. Grundmann, N. N. Ledentsov, *Epitaxy of Nanostructures*, Springer-Verlag, Berlin Heidelberg **2004**.
[4] A. Marent, M. Geller, A. Schliwa, D. Feise, K. Pötschke, D. Bimberg, N. Akçay, N. Öncan, *Appl. Phys. Lett.* **2007**, *91*, 242109.
[5] A. Marent, T. Nowozin, M. Geller, D. Bimberg, *Semicond. Sci. Technol.* **2011**, *26*, 014026.
[6] M. Geller, A. Marent, E. Stock, D. Bimberg, V. I. Zubkov, I. S. Shulgunova, A. V. Solomonov, R. Heitz, D. Bimberg, *Appl. Phys. Lett.* **2006**, *89*, 232105.
[7] T. Müller, F. F. Schrey, G. Strasser, K. Unterrainer, R. Heitz, D. Bimberg, *Appl. Phys. Lett.* **2003**, *83*, 3572.
[8] A. Marent, T. Nowozin, J. Gelze, F. Luckert, D. Bimberg, *Appl. Phys. Lett.* **2009**, *95*, 242114.
[9] M. Geller, Investigation of Carrier Dynamics in Self-Organized Quantum Dots for Memory Devices, Dissertation, Technische Universität Berlin, **2007**.
[10] T. Nowozin, A. Marent, M. Geller, D. Bimberg, N. Akçay, N. Öncan, *Appl. Phys. Lett.* **2009**, *94*, 042108.
[11] C. M. A. Kapteyn, M. Lion, R. Heitz, D. Bimberg, P. N. Brunkov, B. V. Volovik, S. G. Konnikov, A. R. Kovsh, V. M. Ustinov, *Appl. Phys. Lett.* **2000**, *76*, 1573.
[12] J. Bourgoin, M. Lannoo, *Springer Series in Solid-State Sciences*, Vol. 35, Springer, Berlin **1983**.
[13] P. Blood, J. W. Orton, *The Electrical Characterization of Semiconductors: Majority Carriers and Electron States*, Academic, London **1992**.
[14] F. Fan, B. Zhang, Y. Cao, X. Yang, J. Gu, Y. Chen, *Nanoscale* **2017**, *9*, 10610.
[15] J. Gu, N. Li, L. Tian, Z. Lv, Q. Zhang, *RSC Adv.* **2015**, *5*, 36334.
[16] H. Li, Q. Xu, N. Li, R. Sun, J. Ge, J. Lu, H. Gu, F. Yan, *J. Am. Chem. Soc* **2010**, *132*, 5542.
[17] E. E. Mendez, W. I. Wang, B. Ricco, L. Esaki, *Appl. Phys. Lett.* **1985**, *47*, 415.
[18] L. L. Chang, E. E. Mendez, C. Tejedor, *Resonant Tunneling in Semiconductors: Physics and Applications*, Springer, New York **1991**.
[19] R. Tsu, L. Esaki, *Appl. Phys. Lett.* **1973**, *22*, 562.
[20] O. V. Pupysheva, A. W. Dimitriev, A. V. Farajian, H. Mizuseki, Y. Kawazoe, *J. Appl. Phys.* **2006**, *100*, 033718.
[21] M. Tsuchiya, H. Sakaki, *Appl. Phys. Lett.* **1986**, *49*, 88.
[22] M. Tsuchiya, H. Sakaki, *Appl. Phys. Lett.* **1987**, *50*, 1503.
[23] J. Faist, F. Capasso, D. L. Sivco, C. Sirtori, A. L. Hutchinson, A. Y. Cho, *Science* **1994**, *264*, 553.
[24] A. Marent, M. Geller, T. Nowozin, D. Bimberg, *U. S. Patent* **2012**, *8*, 142.
[25] G. Snider, 1D Poisson-Schrödinger Solver, https://www3.nd.edu/gsnider/, **2013**.
[26] S. Datta, *Quantum Transport Atom to Transistor*, C. U. Press (Ed.), Cambridge University Press, **2005**.
[27] R. Lake, S. Datta, *Phys. Rev. B* **1992**, *45*, 6670.
[28] G. L Snider, I. H Tan, E. L Hu, *J. Appl. Phys.* **1990**, *68*, 2849.
[29] T. Nowozin, L. Bonato, A. Högner, A. Wiengarten, D. Bimberg, W. H. Lin, S. Y. Lin, C. J. Reyner, B. L. Liang, D. L. Huffaker, *Appl. Phys. Lett.* **2013**, *102*, 052115.
[30] L. Bonato, E. M. Sala, G. Stracke, T. Nowozin, A. Strittmatter, M. N. Ajour, K. Daqrouq, D. Bimberg, *Appl. Phys. Lett.* **2015**, *106*, 042102.
[31] L. Bonato, I. F. Arikan, L. Desplanque, C. Conion, X. Wallart, Y. Wang, P. Ruterana, D. Bimberg, *Phys. Stat. Sol. (b)* **2016**, *10*, 1877.
[32] M. Geller, E. Stock, C. Kapteyn, R. L. Sellin, D. Bimberg, *Phys. Rev. B* **2006**, *73*, 205331.
[33] I. Vurgaftman, J. R. Meyer, *J. Appl. Phys.* **2001**, *89*, 5815.
[34] G. Stracke, A. Glacki, T. Nowozin, L. Bonato, S. Rodt, C. Prohl, A. Lenz, H. Eisele, A. Schliwa, A. Strittmatter, U. W. Pohl, D. Bimberg, *Appl. Phys. Lett.* **2012**, *101*, 223110.